Articles

Itinerant Ferromagnet $RhFe_3N$: Advanced Synthesis and ^{57}Fe Mössbauer Analysis

Andreas Houben,[†] Vladimir Šepelák,[‡,§] Klaus-Dieter Becker,[‡] and Richard Dronskowski[‡,*]

Institut für Anorganische Chemie, RWTH Aachen University, Landoltweg 1, 52056 Aachen, Germany, and Institut für Physikalische and Theoretische Chemie, Technische Universität Carolo-Wilhelmina zu Braunschweig, Hans-Sommer-Strasse 10, 38106 Braunschweig, Germany

Received November 6, 2008. Revised Manuscript Received January 14, 2009

A novel two-step route for the synthesis of $RhFe_3N$ is presented that yields the target material with a significantly improved phase purity. Except from $Fe_{0.5}Rh_{0.5}$, the absence of other side products is exemplified on the basis of powder XRD, REM/EDX measurements, and Mössbauer investigations. As predicted from density-functional theory calculations, both Rietveld refinement and Mössbauer analysis show that the Rh atom within $RhFe_3N$ exclusively occupies Wyckoff position 1*a* but not 3*c* of the anti-perovskite-like structure in space group $Pm\bar{3}m$, and the rhodium occupation of the 1*a* site is around 80%, yielding a precise formula of $^{1a}(Rh_{0.8}Fe_{0.2})^{3c}(Fe_3)^{1b}N$. The decomposition temperature of the nitride is estimated from temperature-dependent X-ray measurements to lie around 530 °C.

Introduction

Since the invention of magnetic data recording more than a century ago, the capacity of hard discs still doubles every year.[1] The dramatic increase in performance is mostly due to better technologies that rest on fundamental and well-understood physical phenomena such as giant magnetoresistance,[2] but with the exception of conventional magnetic pigments (e.g., γ-Fe_2O_3[3]), the huge potential of solid-state chemistry to contribute to improved data storage has not been fully explored up to the present day. To face this anticipated synthetic challenge,[1] we have focused on the synthesis of nitrogen-containing transition-metal-rich materials, in particular the ternary nitride $RhFe_3N$,[4] because of obvious reasons: with respect to structure and magnetism, $RhFe_3N$ is closely related to the binary nitride γ'-Fe_4N, which has been studied intensively both using experimental[5−7] and theoretical[8,9] methods. This archetypal binary nitride possesses a remarkable chemical inertness and exhibits fascinating magnetic properties that make γ'-Fe_4N a possible material for high-performance magnetic recording heads. In particular, the very large saturation magnetization $M_S = 208$ emu/g (which is close to that of α-Fe with $M_S = 218$ emu/g) and also the low coercive field of $H_C = 5.8$ Oe have attracted early attention.[6] γ'-Fe_4N adopts an anti-perovskite-like crystal structure (Figure 1) with space group $Pm\bar{3}m$ and a lattice parameter of $a = 3.7900(6)$ Å.[7]

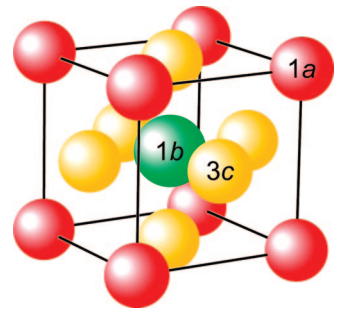

Figure 1. Crystal structure of γ'-Fe_4N in space group $Pm\bar{3}m$ ($a = 3.7900(6)$ Å).[7] The nitrogen atom (green) occupies the very center (Wyckoff position 1*b*), and the iron atoms (red/yellow) are found at the corners (1*a*) and face centers (3*c*). In $RhFe_3N$, the iron atoms at the 1*a* corner positions are almost fully replaced by rhodium atoms.

It is well-known that the magnetic properties of γ'-Fe_4N can be influenced by substituting the iron atoms on Wyckoff positions 1*a* and/or 3*c*. The newly introduced atoms mainly control the crystal growth, thereby yielding magnetic particles with a pronounced anisotropic shape and a high coercive

* Corresponding author. E-mail: drons@HAL9000.ac.rwth-aachen.de. Fax: (49) 241-80-92642.
[†] RWTH Aachen University.
[‡] Technische Universität Carolo-Wilhelmina zu Braunschweig.
[§] On leave from the Slovak Academy of Sciences, Watsonova 45, 04353 Košice, Slovakia.

(1) Albrecht, M.; Thiele, J.-U.; Moser, A. *Phys. J.* **2003**, *10*, 25.
(2) Binasch, G.; Grünberg, P.; Saurenbach, F.; Zinn, W. *Phys. Rev. B* **1989**, *39*, 4828.
(3) Dronskowski, R. *Adv. Funct. Mater.* **2001**, *11*, 27.
(4) Houben, A.; Müller, P.; von Appen, J.; Lueken, H.; Niewa, R.; Dronskowski, R. *Angew. Chem., Int. Ed.* **2005**, *44*, 7212.
(5) Wiener, G. W.; Berger, J. A. *J. Met.* **1955**, *7*, 360.
(6) Chen, S. K.; Jin, S.; Tiefel, T. H.; Hsieh, Y. F.; Gyorgy, E. M.; Johnson, Jr.; D, W. *J. Appl. Phys.* **1991**, *70*, 6247.
(7) Jacobs, H.; Rechenbach, D.; Zachwieja, U. *J. Alloys Compd.* **1995**, *227*, 10.
(8) Matar, S.; Mohn, P.; Demazeau, G.; Siberchicot, B. *J. Phys. (Paris)* **1988**, *49*, 1761.
(9) Kuhnen, C. A.; de Figueiredo, R. S.; Drago, V.; da Silva, E. Z. *J. Magn. Magn. Mater.* **1992**, *111*, 95.

10.1021/cm803004v CCC: $40.75
Published on Web 02/04/2009

field which makes them suitable for high-density storage materials.[10−12] An overview of MFe_3N type ternary nitrides has been given in ref 4.

The substitutional preference of the M atom to go on either Wyckoff position 1*a* and/or 3*c* depends on the relative affinities of Fe or M to the nitrogen atom and, even more important, on the relative sizes of the metallic radii.[13] Only if the metallic radius of the substituting M atom is larger than that of the Fe atom is position 1*a* clearly preferred simply because the coordination sphere of the 1*a*-centered cuboctahedron (see again Figure 1) is much larger than the one of the 3*c* position.[4]

These classical ideas have been corroborated and quantified by quantum-mechanical total-energy calculations from first principles. Our group has also predicted, by means of parameter-free enthalpy calculations based on density-functional theory and the GGA functional, the existence of an enthalpically stable and also ferromagnetic ternary nitride phase, namely $RhFe_3N$, with a formation enthalpy of −7 kJ/mol[14] for the plausible reaction: $FeRh + Fe + FeN \rightarrow RhFe_3N$. The calculations clearly predict that only the 1*a* position of $RhFe_3N$ will be occupied by the rhodium atom.[14]

Shortly after, $RhFe_3N$ was prepared for the first time by two different methods.[4] In particular, we mention the coupled reduction route in analogy to the scheme of Klemm and co-workers,[15,16] where the reduction of a metal oxide is accompanied by the simultaneous formation of an intermetallic alloy. Ternary nitrides such as $RhFe_3N$ are accessible by this method starting with an NH_3:H_2 high-temperature ammonolysis (1:1 ratio) of iron(III) oxide, Fe_2O_3, and elemental rhodium.[4]

Probably because of the small enthalpy of formation (see above) of $RhFe_3N$, its synthesis is always accompanied by the formation of competing phases. At high temperatures, for example, the side-phase $Fe_{0.5}Rh_{0.5}$ ([CsCl]-type, $Pm\bar{3}m$; $a = 2.9825(3)$ Å) is observed. Using the above-mentioned ammonolysis of oxide precursors, the highest $RhFe_3N$ yield (85 wt % or 75 mol %) was achieved at 1100 °C.[4]

Results and Discussion

The novel two-step ammonolysis reaction combines a high-temperature (1100 °C) sintering reaction at temperatures comparable to the previously used coupled reduction reaction with a low-temperature (ca. 500−600 °C) nitriding reaction; the latter temperature may be looked upon as fairly typical for the nitridation of γ'-Fe_4N and related ternary nitrides. A temperature ramp is introduced between the two beforementioned reactions to give the slightly more stable nitride under thermodynamically controlled conditions (see Figure 2). Skipping the sintering reaction resulted in a multiphase mixture of unreacted rhodium, $Fe_{0.5}Rh_{0.5}$ and different binary iron nitrides, somewhat depending on the nitridation temperature. Without the presence of the ramp, the yield decreases significantly.

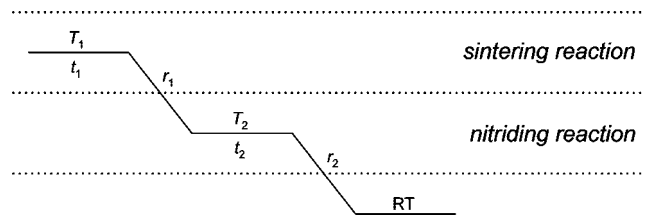

Figure 2. Schematic diagram showing the two-step ammonolysis reaction with a high-temperature (1100 °C) sintering step and a low-temperature (ca. 500−600 °C) nitriding reaction. Between the two reactions, a temperature ramp is introduced to yield the slightly more stable nitride under thermodynamically controlled conditions.

As seen from Figure 3, the use of this strategy allows to maximize the yield of $RhFe_3N$ to up to 94 wt %. In addition, the total reaction time shortens significantly because a regrinding of the intermediately formed metallic precursor is no longer necessary. Thus, the introduction of metal-organic precursors or the often used oxalate precursors can also be circumvented; note that syntheses on the basis of these precursors often suffer from carbidic impurities. We also note that because of the two-step method, the synthesis of many ternary nitrides MFe_3N can be easily accomplished by varying the different synthesis parameters.

The phase and structure determination of $RhFe_3N$ was based on high-resolution X-ray powder diffraction. An aluminum foil was inserted into the X-ray beam line in order to reduce the contribution of Fe fluorescence radiation upon using Cu $K\alpha_1$ radiation. A typical diffraction pattern including the Rietveld refinement is shown in Figure 4.

In accordance with the larger metallic radius of rhodium ($r_{Rh} = 1.34$ Å) compared to iron ($r_{Fe} = 1.24$ Å), the lattice parameter of $RhFe_3N$ ($a = 3.8337(3)$ Å) is also slightly larger — by about 1% — than that of γ'-Fe_4N. Compared to the theoretical prediction by the GGA method ($a = 3.87$ Å), the 1% overestimation of $a(RhFe_3N)$ is characteristic of the here chosen DFT functional.[14,17]

Despite the fact that γ'-Fe_4N and $RhFe_3N$ have very similar lattice parameters, and therefore exhibit characteristic Bragg reflections at very similar scattering angles, the differences in intensities are large enough to prove that γ'-Fe_4N is not at all formed.[4] Additional REM/EDX measurements also evidence that no oxide or carbide phases are present. The absence of crystalline oxide/carbide side phases is also obvious from the X-ray diffraction pattern (see Figure 4).

As predicted from the theoretical calculations,[14] the refinement clearly evidences that among the two possible Wyckoff positions (1*a* and 3*c*) only the 1*a* site is taken by the Rh atom because position 3*c* is just too small for Rh. Nonetheless, it is still possible that position 1*a* is not fully occupied by Rh but also by Fe. Indeed, according to the Rietveld refinement of $RhFe_3N$, Wyckoff position 1*a* is

(10) Andriamandroso, D.; Matar, S.; Demazeau, G.; Fournès, L. *IEEE Trans. Magn.* **1993**, *29*, 2.
(11) Matar, S.; Fournès, L.; ChéRubin-Jeannette, S.; Demazeau, G. *Eur. J. Solid State Inorg. Chem* **1993**, *30*, 871.
(12) Siberchicot, B.; Matar, S. F.; Fournès, L.; Demazeau, G.; Hagenmüller, P. *J. Solid State Chem.* **1990**, *84*, 10.
(13) Cordier-Robert, C.; Foct, J. *Eur. J. Solid State Inorg. Chem* **1992**, *29*, 39.
(14) von Appen, J.; Dronskowski, R. *Angew. Chem., Int. Ed.* **2005**, *44*, 1205; *Angew. Chem.* **2005**, *117*, 1230.
(15) Bronger, W.; Klemm, W. *Z. Anorg. Allg. Chem.* **1962**, *319*, 58.
(16) Schulz, H.; Ritapal, K.; Bronger, W.; Klemm, W. *Z. Anorg. Allg. Chem.* **1968**, *357*, 299.
(17) Perdew, J. P. In *Electronic Structure of Solids*; Ziesche, P., Eschrig, H., Eds.; Akademie Verlag: Berlin, 1991; p 11.

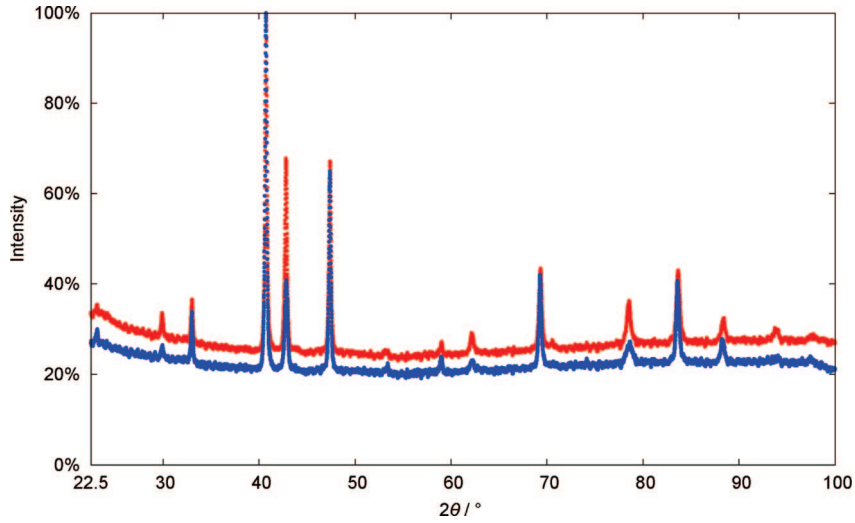

Figure 3. XRD patterns of the products of the two-step synthesis of $RhFe_3N$ (in blue) and the products of the former (coupled reduction) route (in red). As seen from the (110) reflection of $Fe_{0.5}Rh_{0.5}$ at $2\theta = 42.9°$, the molar fraction of the side phase $Fe_{0.5}Rh_{0.5}$ is clearly smaller because of having used the novel route. Note that the total intensity has been standardized for the highest reflection (111) of $RhFe_3N$.

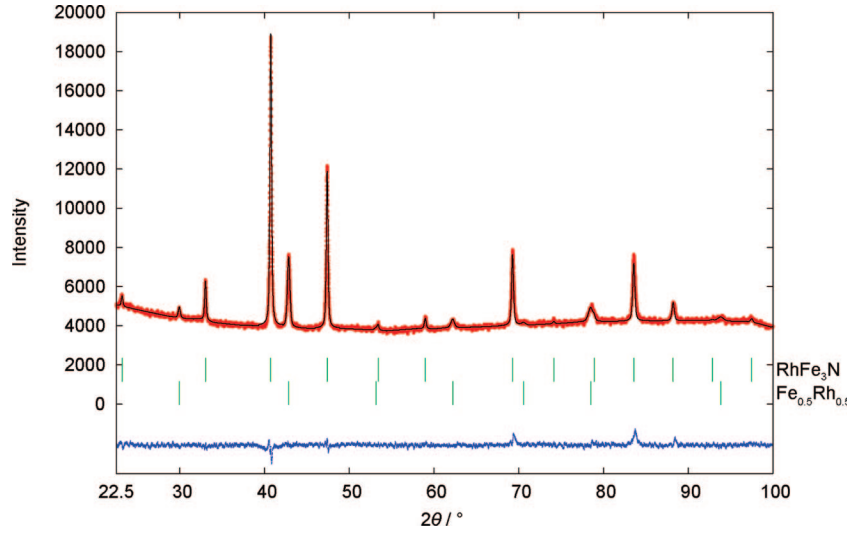

Figure 4. X-ray diffraction pattern and Rietveld refinement of $RhFe_3N$ (first phase: $Pm\bar{3}m$; $a = 3.8337(3)$ Å) and $Fe_{0.5}Rh_{0.5}$ (second phase: [CsCl]-type, $Pm\bar{3}m$; $a = 2.983(1)$ Å). The vertical bars designate the positions of the Bragg reflections.

occupied with Rh (81%) and also Fe (19%) such that the precise formula is $^{1a}(Rh_{0.8}Fe_{0.2})^{3c}(Fe_3)^{1b}N$. For the sake of simplicity, we will nonetheless continue to use the formula $RhFe_3N$ in the sequel. The leftover Rh not used for the synthesis of $RhFe_3N$ forms the binary metallic phase $Fe_{0.5}Rh_{0.5}$ of [CsCl]-type as was denoted before. To study the occupation of Rh and Fe within $RhFe_3N$ and $Fe_{0.5}Rh_{0.5}$ more precisely using a local-probe method, we performed room-temperature ^{57}Fe Mössbauer experiments using two samples from different batches (Figure 5).

Both spectra are nearly identical (therefore, only one is presented) and they are dominated by two sextets of ^{3c}Fe(1) and ^{3c}Fe(2) (see Table 1). The subspectra (^{3c}Fe(1) in green and ^{3c}Fe(2) in blue) can be attributed to the crystallographically (but not spectroscopically) equivalent Wyckoff position 3*c* in $RhFe_3N$. The quadrupole splittings, QS, of these subspectra are the same as those reported for face-centered iron atoms (also at Wyckoff position 3*c*) located on the two

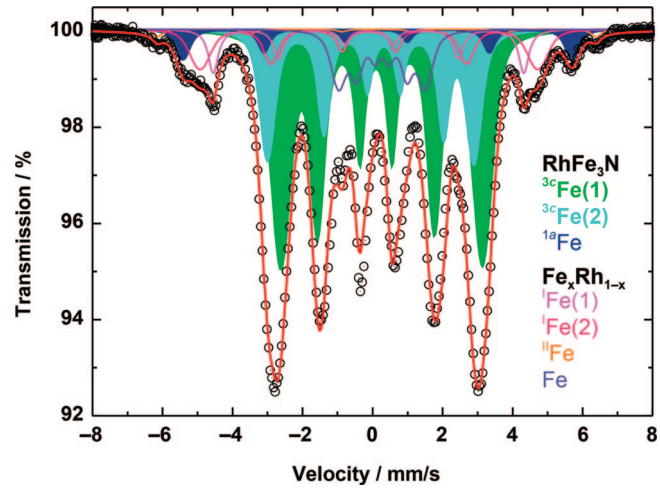

Figure 5. Room-temperature Mössbauer spectra of an as-prepared $RhFe_3N$ sample.

Table 1. Isomer Shifts (IS), Quadrupole Splittings (QS), local Magnetic Fields (B), and Signal Intensities (I) Obtained by Fitting the Room-Temperature Mössbauer Spectra of an As-Received $RhFe_3N$ Sample; Isomer Shifts (IS) are Given Relative to α-Fe[a]

	$RhFe_3N$			Fe_xRh_{1-x}			
	^{3c}Fe(1)	^{3c}Fe(2)	^{1a}Fe	^{I}Fe(1)	^{I}Fe(2)	^{II}Fe	Fe
IS (mm/s)	0.29(2)	0.25(3)	0.24(2)	−0.00(1)	0.01(4)	0.23(1)	0.38(4)
QS (mm/s)	0.08(2)	−0.19(4)	0.01(1)	0.00	0.00	0.00	0.00
B (T)	17.93(3)	18.33(5)	34.01(2)	27.54(2)	29.92(1)	38.94(3)	7.71(3)
I (%)	48.1(1)	22.8(3)	5.0(2)	5.5(2)	8.6(1)	1.0(1)	9.0(2)

[a] Note: 0.29(2) means 0.29 ± 0.02.

corresponding sites in γ′-Fe_4N; for a review see ref.[18] These spectroscopically nonequivalent spectral components arise in the Mössbauer spectra because of the simultaneous presence of magnetic and quadrupolar interactions in the structure. The intensity ratio of both subspectra $I(^{3c}\text{Fe}(1))/I(^{3c}\text{Fe}(2)) \approx 2$ (see Table 1) is in good agreement with expectations based on the crystal structure and magnetism of $RhFe_3N$/γ′-Fe_4N, which indicate that two-thirds of the ^{3c}Fe-atoms experience a quadrupole perturbation of $\text{QS}(^{3c}\text{Fe}(1)) = -eQV_{zz}/8$, whereas the remaining ones experience $\text{QS}(^{3c}\text{Fe}(2)) = eQV_{zz}/4$ (note the opposite signs of the experimentally determined QS values).[18] The values of the hyperfine magnetic fields ($B(^{3c}\text{Fe}(1)) = 17.9$ T, $B(^{3c}\text{Fe}(2)) = 18.3$ T) and of the isomer shifts ($\text{IS}(^{3c}\text{Fe}(1)) = 0.29$ mm/s, $\text{IS}(^{3c}\text{Fe}(2)) = 0.25$ mm/s) of the sextets are slightly reduced in comparison with those characteristic of γ′-Fe_4N ($B(^{3c}\text{Fe}(1)) = 21.5$ T, $B(^{3c}\text{Fe}(2)) = 21.7$ T; $\text{IS}(^{3c}\text{Fe}(1)) = \text{IS}(^{3c}\text{Fe}(2)) = 0.31$ mm/s).[18] The reduced local magnetic fields acting on the ^{3c}Fe atoms in the investigated materials are due to the lower value of the magnetic moment of the Rh atom in comparison with that of the Fe atom.[19] Note that Rh on the 1*a* site is the nearest neighbor to iron located on the 3*c* sites. Additionally, the substitution of Fe by Rh in γ′-Fe_4N could also result in a change of the electron density around the iron nuclei, leading to lower values of the isomer shifts.

There is one additional subspectrum (Figure 5, in dark blue) whose parameters ($\text{IS}(^{1a}\text{Fe}) = 0.24$ mm/s, $\text{QS}(^{1a}\text{Fe}) = 0.01$ mm/s, $B(^{1a}\text{Fe}) = 34$ T, $I(^{1a}\text{Fe}) = 5.0\%$) are almost identical to those characteristic of iron atoms occupying the corners (1*a* sites) in the structure of γ′-Fe_4N ($\text{IS}(^{1a}\text{Fe}) = 0.24$ mm/s, $\text{QS}(^{1a}\text{Fe}) = 0$ mm/s, $B(^{1a}\text{Fe}) = 33.9$ T).[18] Therefore, this subspectrum can be attributed to Fe atoms on 1*a* sites in $RhFe_3N$. Note that the nearest neighbors of these Fe atoms are Fe, just like in γ′-Fe_4N. In the latter phase, the intensities ratio of the ^{1a}Fe, ^{3c}Fe(1), and ^{3c}Fe(2) sites is given by $I(^{1a}\text{Fe}):I(^{3c}\text{Fe}(1)):I(^{3c}\text{Fe}(2)) = 1:2:1$.[18] For $RhFe_3N$, the intensity ratio $I(^{1a}\text{Fe}):I(^{3c}\text{Fe}(1)):I(^{3c}\text{Fe}(2))$ of about 0.21:2.1:1, obtained by fitting the present Mössbauer spectra, indicates that about 80% of the 1*a* sites are occupied by Rh. This is in excellent agreement with the occupation value resulting from the Rietveld refinement.

The highest hyperfine magnetic field identified in the spectra is $B(^{II}\text{Fe}) = 38.9$ T. Mössbauer studies of Fe_xRh_{1-x} alloys have shown that such a large hyperfine field is characteristic for Fe_xRh_{1-x} alloys with $x > 0.5$.[20] It was also shown that in this compositional range, the Mössbauer spectrum of Fe_xRh_{1-x} consists of two sextets: the first one

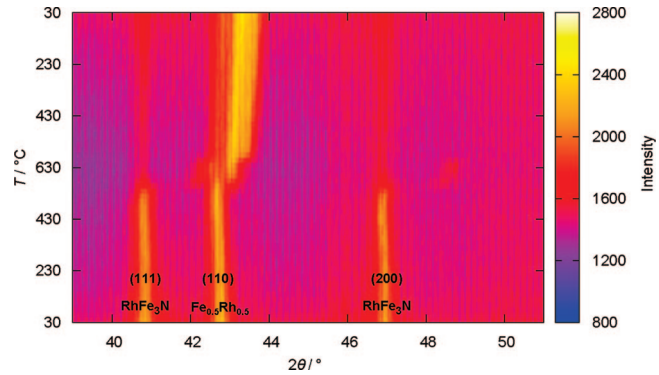

Figure 6. Temperature-dependent X-ray diffraction of $RhFe_3N$ and $Fe_{0.5}Rh_{0.5}$ in the 2θ range between 39 and 51°; three individual reflections have been indicated. The nitride is stable up to a temperature of approximately 530 °C and decomposes at higher temperatures. Note that the graph shows a heating and a subsequent cooling step.

corresponds to iron atoms (denoted as ^{II}Fe) possessing identical nearest neighbors, namely 8 iron (^{I}Fe) atoms. The second sextet is associated with the ^{I}Fe atoms surrounded by ^{II}Fe and Rh as nearest neighbors. The subspectrum with $B(^{II}\text{Fe}) = 38.9$ T is thus attributable to ^{II}Fe in Fe_xRh_{1-x}. The intensity of the spectral component assigned to ^{II}Fe was found to decrease with increasing Rh concentration and disappears at $x = 0.5$ (for $x < 0.5$, the Mössbauer spectrum of Fe_xRh_{1-x} alloys exhibits only one sextet).[20]

In line with this, the other spectral components found in the spectra of both samples could be assigned to Fe_xRh_{1-x} phases with at least 3 different values of x. The spectral components with the relatively large hyperfine fields of $B(^{I}\text{Fe}(1)) = 27.5$ T and $B(^{I}\text{Fe}(2)) = 29.9$ T correspond to ^{I}Fe atoms in Fe_xRh_{1-x} with $x > 0.5$. On the other hand, the component denoted by Fe with a relatively small hyperfine field ($B(\text{Fe}) \approx 8$ T) can be associated with Fe atoms in Fe_xRh_{1-x} with $x < 0.5$. Generally, all the Mössbauer parameters of Fe_xRh_{1-x} phases obtained by fitting the spectra of both samples (see Table 1) are in good agreement with those reported in the literature.[20] Nonetheless, we mention a small discrepancy between the fit and the experimental spectrum around a velocity of $v = 0$ mm/s. This may be explained by the further presence of a small admixture of the γ-phase of Fe_xRh_{1-x}, which is formed in a wide composition and temperature range, and could also be formed during high-temperature synthesis.

Finally, temperature-dependent X-ray diffraction experiments were carried out up to 630 °C to determine the decomposition temperature of $RhFe_3N$. As can be seen from Figure 6, the decomposition starts at about 530 °C and is completed at about 570 °C. Within this temperature range, the $RhFe_3N$ reflections start to disappear while the $Fe_{0.5}Rh_{0.5}$

(18) Bartels, O.; Becker, K. D. *Z. Phys. Chem.* **2007**, *221*, 1509.
(19) Wu, Z.; Meng, J. *Appl. Phys. Lett.* **2007**, *90*, 241901.
(20) Shirane, G.; Chen, C. W.; Flinn, P. A. *Phys. Rev.* **1963**, *131*, 183.

reflection drastically broadens. The latter phenomenon also demonstrates that the Fe_xRh_{1-x} phase covers a broad range of x values (see above). In this case, the decomposition process of $RhFe_3N$ with the given stoichiometry is the reason for the broad range of compositions. The reformation of the ternary phase was not observed while recooling the sample to lower temperatures.

Conclusion

A significantly improved route for synthesizing the ternary iron rhodium nitride $RhFe_3N$ was devised by applying a two-step method with product yields of up to 94 wt %. The absence of oxidic or carbidic impurities was shown from EDX and XRD analysis. Rietveld refinements of the X-ray patterns in combination with Mössbauer experiments prove that the Rh atom in $RhFe_3N$ exclusively occupies Wyckoff position 1*a*, just as predicted by density-functional theory. Also, both independent methods evidence a high Rh occupation (ca. 80%) of the 1*a* site, to be compared with many other ternary MFe_3N nitrides.[4,14] According to this, the precise formula is $^{1a}(Rh_{0.8}Fe_{0.2})^{3c}(Fe_3)^{1b}N$. In addition, the experimental data also show the absence of other concurrent phases such as γ'-Fe_4N. The decomposition temperature of the nitride is determined to be around 530 °C.

Experimental Section

Synthesis. The powdered reactants Rh and Fe_2O_3 were mixed and accurately ground using a stoichiometric ratio of 1:3 for the metal atoms. For the optimized synthesis the following parameters (see Figure 2) were used: $T_1 = 1100$ °C, $t_1 = 2$ h, $T_2 = 500$ °C, $t_2 = 4$ h. The ammonolysis gas was a NH_3:H_2 mixture with a 1:1 ratio.

XRD and Rietveld Refinement. X-ray diffraction at room temperature was performed using a calibrated Huber G670 Image plate powder diffractometer with Cu $K\alpha_1$ radiation ($\lambda = 1.54059$ Å; flat sample; $5 \leq 2\theta \leq 100°$; step rate 0.005° in 2θ). The Rietveld refinement was carried out with the program FullProf[21] and a pseudo-Voigt profile function with a Gaussian-Lorentz η mixing parameter of 0.6(2). The residual values for $RhFe_3N$ are $R_p = 0.0152$ and $R_B = 0.112$ for 14 Bragg reflections (19001 data points) and 11 refined parameters. The positions are 1*a* for Rh, 1*b* for N and 3*c*/1*a* for Fe within space group $Pm\bar{3}m$. The formula weight is $M = 284.45$ g/mol with a cell volume of $V = 56.345(6)$ Å^3. The X-ray density is $\rho = 8.38$ g/cm^{-3}. The refined lattice parameter of $RhFe_3N$ is $a = 3.8337(3)$ Å. By constraining the sum of the occupation parameters of iron and rhodium on 1*a* to unity, the rhodium contribution for this position arrived at 81%. Likewise, the iron occupation on position 3*c* was refined to be 100%. The second phase is $Fe_{0.5}Rh_{0.5}$ which adopts a [CsCl]-type structure ($Pm\bar{3}m$) with a lattice parameter of $a = 2.983(1)$ Å.

REM/EDX. We used a LEO Supra 35VP (LEO Electron microscopy, Cambridge) for the REM and an INCA Energy 200 (Si(Li)-crystal) from Oxford Instruments for the EDX analysis.

Mössbauer. Mössbauer spectra of two samples from different batches were taken in transmission geometry at room temperature. A ^{57}Co/Rh γ-ray source was used. The velocity scale was calibrated relative to ^{57}Fe in α-Fe. Recoil spectral analysis software[22] was used for the quantitative evaluation of the Mössbauer spectra.

Acknowledgment. We thank Dr. Paul Müller for having performed the temperature-dependent X-ray measurements, Dr. Michael Noyong for the REM/EDX analysis, Dr. Roland Winde (Umicore, Wolfgang Hanau) for the kind supply of metallic rhodium, and Deutsche Forschungsgemeinschaft for having funded this study. V.Š. thanks APVV (Project 0728-07) and VEGA (2/0065/08) for the support of his work.

CM803004V

(21) Rodriguez-Carvajal, J. *FULLPROF version 4.0*; Institut Laue-Langevin: Grenoble, France, 2007.
(22) Lagarec, K.; Rancourt, D. G. *Recoil - Mössbauer Spectral Analysis Software for Windows, version 1.02*; Department of Physics, University of Ottawa: Ottawa, ON, 1998.